JMEPEG (2005) 14:495-502
DOI: 10.1361/105994905X56214

1059-9495/$19.00

Laser Shock Processing Induced Residual Compression: Impact on Predicted Crack Growth Threshold Performance

M.J. Shepard

(Submitted November 12, 2004; in revised form April 5, 2005)

Design credit is not currently taken for laser shock processing (LSP) induced compressive residual stresses in damage tolerant design. The inclusion of these and other compressive stresses in design practice has the potential to dramatically increase predicted fatigue crack growth threshold performance and damage tolerant design life. In the current effort, Ti-6Al-4V coupons will be subjected to shot peening, glass bead peening, and high intensity laser shock processing. The in-depth residual stresses due to processing will be analyzed and then input into a linear elastic fracture mechanics analysis code to predict fatigue crack growth threshold performance. This analysis establishes both the utility and feasibility of incorporating LSP-induced compressive residual stresses into damage tolerant design practice.

Keywords crack growth, design, fatigue, laser shock processing, residual stress

1. Introduction

Compressive residual stresses have long been known to have the potential to increase the fatigue and fatigue crack growth resistance of metallic structures. In many aerospace applications residual stress inducing surface treatments, primarily shot peening, are often applied to increase the margin of safety in an effort to avoid fatigue failure. In this context, the beneficial effects of residual stresses on fatigue performance are not accounted for in the design. Therefore, the design is not reliant on the presence of a particular magnitude of induced compressive residual stress. The residual compression is imparted strictly to increase the factor of safety.

This failure to account for the beneficial compressive residual stresses in design is due to a number of factors. First, no generally accepted, non-destructive, residual stress measurement technique is currently available to determine in-depth residual stress profiles. Consequently, any resulting design would have to proceed based on an assumed residual stress distribution. Any design that included credit for induced compressive stresses would have to enter service with no independent verification that one critical component of the design (a given in-depth compressive stress state) was present. Since shot peening, currently the most pervasive surface treatment technology, is inherently a chaotic process, even rigorous process control measures may not be sufficient to guarantee a given residual stress profile in a given component, particularly after service-induced redistribution. Second, until recently, induced compressive residual stresses were typically of a fairly shallow depth, limited to what could be induced by conventional shot peening. As an example, in Ti-6Al-4V, shot peening induced compression would be expected only to nominal depths between 0.1 and 0.15 mm, depending on peening conditions. While high magnitude compression to these depths can be expected to provide a very useful life benefit, the potential exists for either "loss" of this shallow compressive layer or for flaws larger than originally envisioned in the design.

Third, surface treatment techniques can potentially introduce undesirable artifacts in the treated surface. In the case of shot peening, this is due to the repeated impact of the shot. These artifacts can take the form of subtle stress concentrations due to increased surface roughness, extensive shear banding and localized plasticity, and even crack-like defects (Ref 1-3). In many instances these artifacts are either benign or are non-critical since they are embedded in high magnitude compressive stresses. However, in other instances these artifacts can act to decrease fatigue life below that of an unshot-peened baseline condition (Ref 4, 5).

With these three factors in mind, it would be desirable if an alternative to conventional shot peening existed that was more amenable to real-time process control, induced deeper compressive residual stresses, and was less likely to induce subtle artifacts that might be difficult to detect and yet act to reduce fatigue strength. Fortunately, several such approaches exist. Among these processes is laser shock processing (LSP), which is currently used in some turbine engine fan and compressor hardware to reduce sensitivity to foreign object damage (FOD) and fretting fatigue (Ref 6-8).

In the case of laser peened fan blades, the designs have not been reliant on the residual stresses induced by laser peening. In other words, without in-service damage, the blades should not fail. LSP is applied strictly to increase the size of damage that the blade can sustain in-service without failing. Not only does this increase the durability of the design, increases in the damage tolerance of leading edges can provide significant savings in terms of reduced maintenance costs from the relaxation of inspection requirements and increased size of FOD necessitating immediate corrective action.

M.J. Shepard, Air Force Research Laboratory, Materials and Manufacturing Directorate, Wright-Patterson Air Force Base, OH 45433-7817. Contact e-mail: michael.shepard@wpafb.af.mil.

Currently, many expensive turbine engine components are life limited by projected crack growth of small, difficult to detect flaws at a few critical locations. In some instances, component lives could be extended 50-100% if crack growth resistance or threshold performance could be improved in one or more of the life-limiting features.

It is proposed that through careful process control and selection of design methods it may be possible to take damage tolerant design life credit for the increased threshold crack growth performance and eventually, lower crack growth rates in regions containing deep compressive residual stresses, such as those induced by laser peening.

Although other methods of imparting deep compressive residual stresses are available, this preliminary study will focus on laser shock processing induced compressive stresses. Predictions made accounting for LSP induced compressive residual stresses should be indicative of the results that might be obtained with other processes capable of inducing deep compressive residual stresses.

2. Experimental Methods

2.1 Specimens

Simple 12.7 mm thick disk-type specimens were sectioned from 50.8 mm diameter Ti-6Al-4V (wt.%) bar stock for use in the determination of surface treatment induced compressive residual stresses. These specimens were wafered from the bar stock using wire electrical discharge machining (wire EDM). The recast layer associated with wire EDM was removed by low stress grind to final thickness and an 0.2 μm surface finish. A small notch, oriented parallel with the final polishing marks, was cut at the edge of one side of each specimen with a key file. These small notches provided differentiation between the two sides of the specimen and provided a rotational reference. The disk-type specimen geometry was selected because it provides radial symmetry with respect to the circular laser shock applied at the center of the specimen.

The Ti-6Al-4V bar stock used for this experiment was hot-rolled to near dimension and then mill annealed. The bar stock was centerless ground to final dimension. The material was in conformance with the AMS 4928Q specification for bars, wire, forgings, rings, and drawn shapes in annealed Ti-6Al-4V.

Ti-6Al-4V is a widely used $\alpha + \beta$ Ti alloy that is frequently employed due to its generally good combination of strength, fatigue, and creep properties at room and moderately elevated temperature. Ti-6Al-4V is commonly employed in fan and compressor hardware in turbine engines due not only to its good combination of properties, but also due to the economies derived from its pervasive use.

After machining, all specimens were subjected to a stress relief anneal to minimize residual stresses due to prior processing. This ensured that the documented residual stresses would be due to the applied surface treatments rather than to previous processing or machining steps. Specimens were wrapped in tantalum foil and heat treated under vacuum to preclude the formation of any alpha case. The thermal excursion consisted of a one hour ramp up to 704 °C, 1 h hold at temperature, and a furnace cool to room temperature.

Post stress relief anneal surface residual stresses were determined for a number of specimens using x-ray diffraction (XRD) residual stress analysis. All stresses were found to be near zero, but slightly compressive, with no measurement exceeding −11 MPa. Two subsurface measurements were also near zero and slightly compressive.

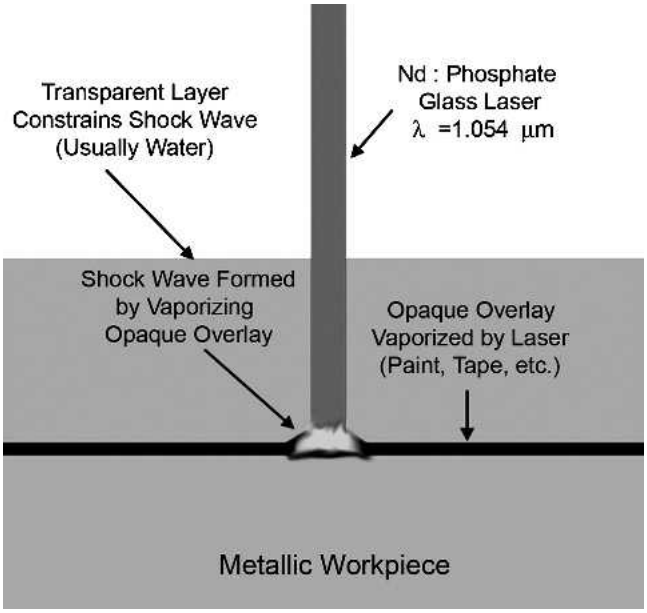

Fig. 1 Schematic illustration of laser shock peening process

2.2 Surface Treatments

LSP, also known as laser shock peening, or any of several trade names, such as the LaserPeen process or Lasershot peening, is primarily a method for introducing deep (often >1 mm) compressive residual stresses into the surfaces of components. In the process, a laser beam is used to vaporize a thin opaque coating (or absorber) applied to the surface of the component. The vaporization of the opaque coating produces a rapidly expanding plasma confined against the surface of the component by a constraining layer (tamping) largely transparent to the laser wavelength being used for processing. This constraint of the rapidly expanding plasma causes a shock wave to pass into the material.

If this shock wave is of sufficient magnitude, the peak pressures will exceed the Hugoniot elastic limit (dynamic yield stress under shock conditions) of the material and the shocked region will undergo plastic deformation. After the shock wave dissipates, the plastically deformed region is left in a state of residual compression due to constraint from the surrounding undeformed material. As a result, offsetting tensile stresses are found outside the processed regions. The LSP process is shown schematically in Fig. 1. Further details on the LSP process can be found elsewhere (Ref 9-11).

All LSP was conducted at LSP Technologies in Dublin, OH. Any application of laser shock processing to enhance design life would operate on the deepest, highest magnitude state of compression that could be developed without causing related problems such as unacceptable distortion or dangerously high magnitude tensile compensatory residual stresses. As such, the conditions selected for study could be considered "high-intensity" LSP conditions. A single spot was laser shocked three times in the center of each 50.8 mm diameter disk with a laser power density of 8 GW/cm^2 and laser pulse duration of 20 ns.

A Q-switched neodymium doped phosphate glass laser was used for all laser shock processing. The characteristic radiation from this system has a wavelength of 1.054 μm, in the near-infrared regime. The diameter of the laser shock was held at 5.3 mm for all experiments. The opaque and transparent overlays were flat black vinyl tape and flowing water, respectively. Laser shocks were applied simultaneously to both sides of the specimen, a technique that has been used historically to minimize distortion of fan blade leading edges.

To provide a reference residual stress state representative of turbine engine hardware, shot peening induced residual stresses were also investigated. Shot peening was conducted at Metal Improvement Company in Blue Ash, OH. Specimens were peened to 6-8A Almen intensity with S170R cast steel shot and 6-9N Almen intensity with number 5 glass beads. Coverage was fixed at 125%. Both these peening conditions are commonly used for titanium alloy turbine engine hardware.

2.3 X-ray Diffraction Residual Stress Analysis

The XRD technique for residual stress analysis is a well-documented approach for estimating residual stresses in relatively isotropic crystalline solids. In this technique, Bragg's Law is used to determine strains in the crystalline lattice. Residual stresses are then inferred from these strains based on knowledge of the x-ray elastic constants for the interrogated crystallographic plane and a model for the stress state in the measured region. An excellent description of the most widely employed techniques can be found in SAE HS-784 (Ref 12). A number of other references are available (Ref 13, 14).

In-depth residual stress analysis was conducted for each surface treatment at Lambda Research in Cincinnati, OH. After verification that the lattice spacing was a linear function of $\sin^2\psi$ as required for the plane stress linear elastic residual stress model (Ref 12-15), XRD residual stress measurements were made employing a $\sin^2\psi$ technique and the diffraction of $CuK_{\alpha 1}$ radiation from the (21.3) planes of the alpha phase.

For subsurface measurements, material was removed electrolytically to prevent the alteration of the subsurface residual stress distributions due to mechanical material removal. The in-depth residual stress analysis results were corrected for both the penetration of the radiation into the subsurface stress gradient (Ref 16) and for any stress relaxation caused by the electrolytic removal of stressed material (Ref 17).

X-ray elastic constants required to calculate the macroscopic residual stress from the strain normal to the (21.3) planes of the alpha phase were determined in accordance with ASTM E1426-91. Systematic errors were monitored per ASTM specification E915.

2.4 Linear Elastic Fracture Mechanics (LEFM) Analysis

In an effort to assess the effect of residual stresses associated with LSP on fatigue behavior, calculations of the threshold condition for assumed flaws embedded in the experimentally determined residual stress fields were made using a linear elastic fracture mechanics routine created and exercised in MATLAB, published by Mathworks, Inc. The calculations used an approximate K solution developed by Wang (Ref 18) for a surface flaw subjected to an arbitrary stress field based on the weight function method as proposed by Shen and Glinka (Ref 19). The reference stress intensity factor solutions for the weight function analysis were taken from the finite element modeling work of Shiratori (Ref 20) and the work collected:

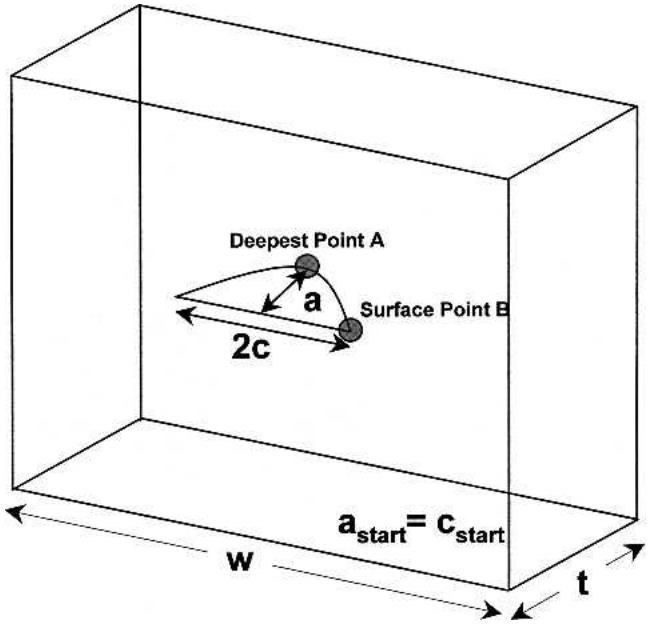

Fig. 2 Schematic illustration of selected LEFM geometry

$$K = \int_0^a \sigma(x) m(x,a,a/c,a/t)\,dx \qquad \text{(Eq 1)}$$

by Murakami and co-workers (Ref 21). A schematic illustration of the modeled geometry can be found in Fig. 2.

In this approach stress intensity factor, K is approximated by Eq 1. Different weight functions, $m(x,a,a/c,a/t)$, are used for the subsurface point A and the surface point B (Fig. 2) and are denoted m_A and m_B, respectively. These weight functions for the subsurface point and surface point are defined as follows:

$$A_0 = 1.13047 - 0.12945\left(\frac{a}{c}\right) + 0.03526\left(\frac{a}{c}\right)^2$$

$$A_1 = 1.08461 - 1.01106\left(\frac{a}{c}\right) + 0.2454\left(\frac{a}{c}\right)^2$$

$$A_2 = 0.7855 + 0.5517\left(\frac{a}{c}\right) - 0.0934\left(\frac{a}{c}\right)^2$$

and

$$Y_1 = B_0 + B_1\left(\frac{a}{t}\right)^2 + B_2\left(\frac{a}{t}\right)^4$$

$$B_0 = 0.5044 - 0.2609\left(\frac{a}{c}\right) + 0.0529\left(\frac{a}{c}\right)^2$$

$$B_1 = 0.7259 - 0.6352\left(\frac{a}{c}\right) + 0.1492\left(\frac{a}{c}\right)^2$$

$$B_2 = -0.6459 + 0.4177\left(\frac{a}{c}\right) - 0.0731\left(\frac{a}{c}\right)^2$$

$$m_A(x,a) = \frac{2}{\sqrt{2\pi(a-x)}}\left[1 + M_{1A}\left(1-\frac{x}{a}\right)^{1/2} + M_{2A}\left(1-\frac{x}{a}\right) + M_{3A}\left(1-\frac{x}{a}\right)^{3/2}\right]$$

where

$$M_{1A} = \frac{2\pi}{\sqrt{2Q}}(2Y_0 - 3Y_1) - \frac{24}{5}$$

$$M_{2A} = 3$$

$$M_{3A} = \frac{6\pi}{\sqrt{2Q}}(2Y_1 - Y_0) - \frac{8}{5}$$

$$Q = \begin{cases} 1 + 1.464\left(\frac{a}{c}\right)^{1.65} & \text{for } 0 \le \frac{a}{c} \le 1.0 \\ \left[1 + 1.464\left(\frac{c}{a}\right)^{1.65}\right]\left(\frac{a}{c}\right)^2 & \text{for } \frac{a}{c} > 1.0 \end{cases}$$

$$Y_0 = A_0 + A_1\left(\frac{a}{t}\right)^2 + A_2\left(\frac{a}{t}\right)^4 \qquad \text{(Eq 2)}$$

$$m_B(x,a) = \frac{2}{\sqrt{2\pi(a-x)}}\left[1 + M_{1B}\left(1-\frac{x}{a}\right)^{1/2} + M_{2B}\left(1-\frac{x}{a}\right) + M_{3B}\left(1-\frac{x}{a}\right)^{3/2}\right]$$

$$M_{1B} = \frac{3\pi}{\sqrt{Q}}(5F_1 - 3F_0) - 8$$

$$M_{2B} = \frac{15\pi}{\sqrt{Q}}(2F_0 - 3F_1) + 15$$

$$M_{3B} = \frac{3\pi}{\sqrt{Q}}(10F_1 - 7F_0) - 8$$

$$Q = \begin{cases} 1 + 1.464\left(\frac{a}{c}\right)^{1.65} & \text{for } 0 \le \frac{a}{c} \le 1.0 \\ \left[1 + 1.464\left(\frac{c}{a}\right)^{1.65}\right]\left(\frac{a}{c}\right)^2 & \text{for } \frac{a}{c} > 1.0 \end{cases}$$

$$F_0 = \left[C_0 + C_1\left(\frac{a}{t}\right)^2 + C_2\left(\frac{a}{t}\right)^4\right]\sqrt{\frac{a}{c}}$$

$$C_0 = 1.133469 - 0.29091\left(\frac{a}{c}\right) + 0.08125\left(\frac{a}{c}\right)^2$$

$$C_1 = 1.757673 - 1.5275\left(\frac{a}{c}\right) + 0.37185\left(\frac{a}{c}\right)^2$$

$$C_2 = 0.08429 + 0.4423\left(\frac{a}{c}\right) - 0.1894\left(\frac{a}{c}\right)^2$$

and

$$F_1 = \left[D_0 + D_1\left(\frac{a}{t}\right)^2 + D_2\left(\frac{a}{t}\right)^4\right]\sqrt{\frac{a}{c}}$$

$$D_0 = 0.11855 - 0.2065\left(\frac{a}{c}\right) + 0.07817\left(\frac{a}{c}\right)^2$$

$$D_1 = 1.15312 - 0.98743\left(\frac{a}{c}\right) + 0.23315\left(\frac{a}{c}\right)^2$$

$$D_2 = -0.2246 + 0.4784\left(\frac{a}{c}\right) + 0.1864\left(\frac{a}{c}\right)^2 \qquad \text{(Eq 3)}$$

The total stress intensity factor due to applied and residual stresses may be found via superposition provided that the total stresses are assumed to be elastic.

A sigmoidal expression (Eq 4) was used to relate calculated stress intensity factor range ΔK to crack growth rate at the deepest point da/dN and at the surface dc/dN (Ref 22). Constants for Eq 4 were taken from the final report of the National High Cycle Fatigue Program and are tabulated in Table 1 (Ref 22). Continuous expressions for the residual stress:

$$da/dN = e^B\left(\frac{K_{eff}}{K_{th}}\right)^P\left[\ln\left(\frac{K_{eff}}{K_{th}}\right)\right]^Q\left[\ln\left(\frac{K_c}{K_{eff}}\right)\right]^d \qquad \text{(Eq 4)}$$

where

$$K_{eff} = K_{max}(1-R)^m = \Delta K(1-R)^{(m-1)} \qquad \text{(Eq 5)}$$

states as a function of depth were developed based on the recommendations of VanStone as reported by Tuft (Eq 6) (Ref 23). Equation 6 provides excellent fits for shot-peened data. A slight modification of this form (Eq 7) was found to provide a much more accurate representation of LSP induced stresses, where the subsurface stresses do not approach zero rapidly.

$$\sigma_{rs}(x) = A_1 e^{\left(\frac{-x}{\lambda}\right)}\sin(B_1 x + C_1) \qquad \text{(Eq 6)}$$

$$\sigma_{rs}(x) = A_1 e^{\left(\frac{-x}{\lambda}\right)}\sin(B_1 x + C_1) + D_1 \qquad \text{(Eq 7)}$$

The methods described previously were adopted because of their general applicability to arbitrary stress fields and their computational efficiency. However, the author recognizes the limitations of the selected methods. First, surface crack growth is almost completely suppressed due to the high magnitude

Table 1 Constants for Crack Growth Eq 1 and 2 from Ref 23

Constant	Value(a)
Kth	3.829
P	3.7107
d	–0.0066
m+	0.72
B	–18.144
Q	0.2349
Kc	60
m–	0.275

(a) English units

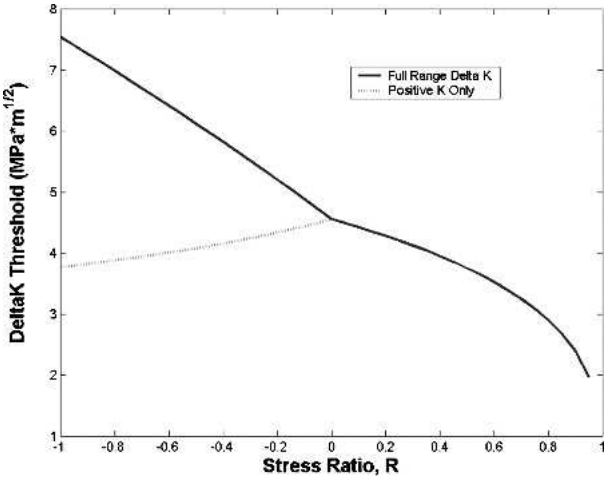

Fig. 3 Threshold stress intensity factor range versus stress ratio

compressive stresses at the surface. This in turn leads to cracks that grow to *a/c* ratios greater than 2. At these higher *a/c* ratios, this weight function solution becomes inaccurate for prediction of the actual stress intensity factor ranges at the surface point B and the deepest point A. Additionally, the total stress ratio, combining the residual and applied stresses, used to calculate the crack growth rate, can be highly negative for some combinations of applied and compressive residual stresses, <−10 in some cases. No data were available for stress ratios <−1 to verify that the sigmoidal crack growth expression would provide reasonable estimates of crack growth rates. Because of the iterative nature of life prediction algorithms any errors due to these factors could be continuously compounded throughout the prediction, leading to significant errors in the life prediction.

Although the above approach can be used for preliminary life prediction (cycles to failure), no results for such calculations are presented due to the limitations of the current approach. Rather, a design to threshold approach was adopted. In such an approach, for a given flaw size, at a given applied stress ratio, the maximum uniform sectional stress that could be applied with no crack growth is calculated.

3. Results and Discussion

3.1 Threshold Modeling

Threshold values were estimated by using Eq 4 and 5 to estimate the stress intensity factor range at which crack growth was predicted to be 2.54×10^{-7} mm/cycle. The convention using only the positive portion of the stress intensity factor range was employed. This convention diverges from the full range definition of ΔK at stress ratios R of less than zero. Threshold predictions utilizing both conventions are presented in Fig. 3. Threshold values were limited to 3.77 MPa $\sqrt{m}$ at and below $R = -1$, and 1.97 MPa $\sqrt{m}$ as R approached 1. The threshold stress intensity factor reaches a maximum of 4.56 MPa $\sqrt{m}$ around $R = 0$. This range between $R = -1$ and $R = 0.95$ entails the entire range of stress ratios where reliable crack growth threshold data exists (Ref 22).

Development of more advanced methods supporting arbitrary three-dimensional crack growth are being pursued, but these methods are typically computationally expensive, and thus unsuited to the current research. Since the objective of the current study is to explore the magnitude of benefit from LSP induced compressive residual stresses for many different flaw sizes, the use of a threshold analysis is considered adequate. For predictions of greater fidelity the more computationally intensive techniques should be considered (Ref 24, 25).

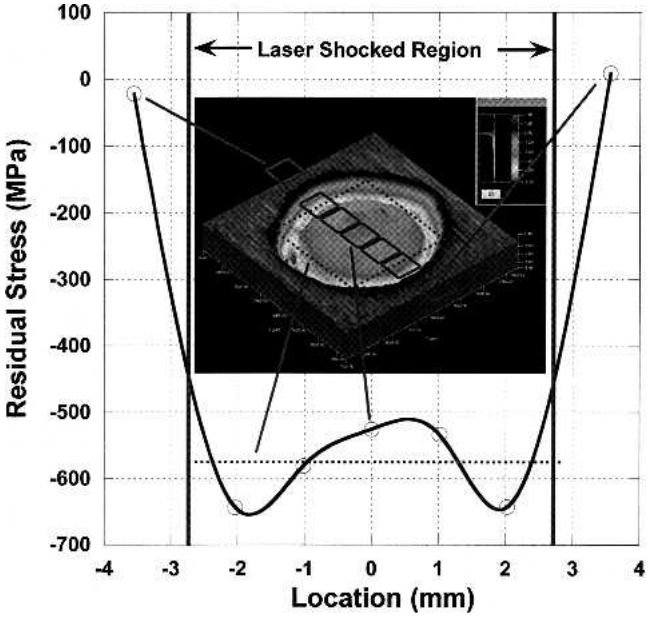

Fig. 4 Map of residual stress analysis results across a laser-shocked region

3.2 Residual Stresses

3.2.1 Variations in Residual Stress Inside Laser Shocked Region. Figure 4 depicts graphically an experiment in which the LSP induced surface stresses were mapped along a line running across the diameter of a laser shocked region. The irradiated regions were 1 mm square. Seven measurements were made across the shocked region; five across the shock and one on each side of the shock. The residual stress component tangential to the circumference of the laser shock was measured. The trend line in Fig. 4 is simply intended to aid the eye and no physical significance is implied.

The residual stresses determined in the laser-shocked region were all compressive, with the highest stresses observed in the annular region at the edge of the shock. The magnitude of the compression in the center of the shock was somewhat lower than that observed in the edge regions. Residual stresses measured outside of the laser-shocked region were compressive and near zero, but trended toward the tension anticipated outside of the shocked region. Other results from the literature show similar trends (Ref 26, 27).

A measurement using a larger (3 × 3 mm) irradiated region covering the majority of the shocked region is depicted as a dotted line in Fig. 4. The residual stress estimates derived from XRD residual stress analysis should represent the average stress in the irradiated region. Assuming the residual stresses in the shocked "circle" exhibit the expected radial symmetry, this measurement is in excellent agreement with the measurements made using smaller irradiated regions.

This result is extremely useful since XRD experiments us-

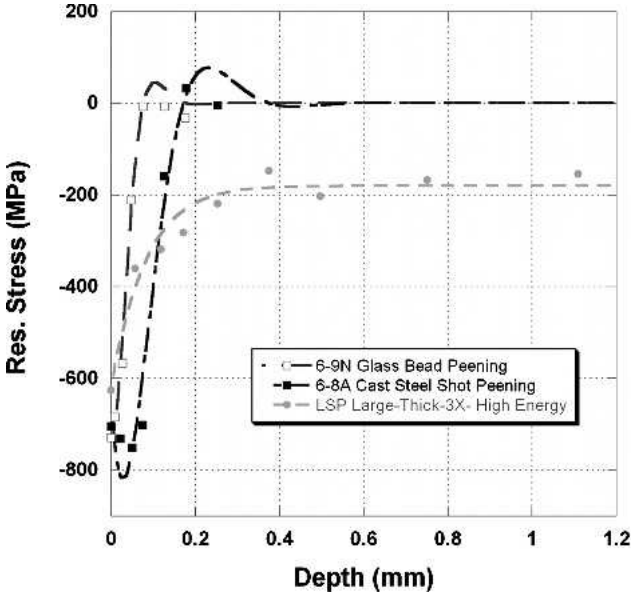

Fig. 5 In-depth residual stress profiles used for LEFM threshold analysis

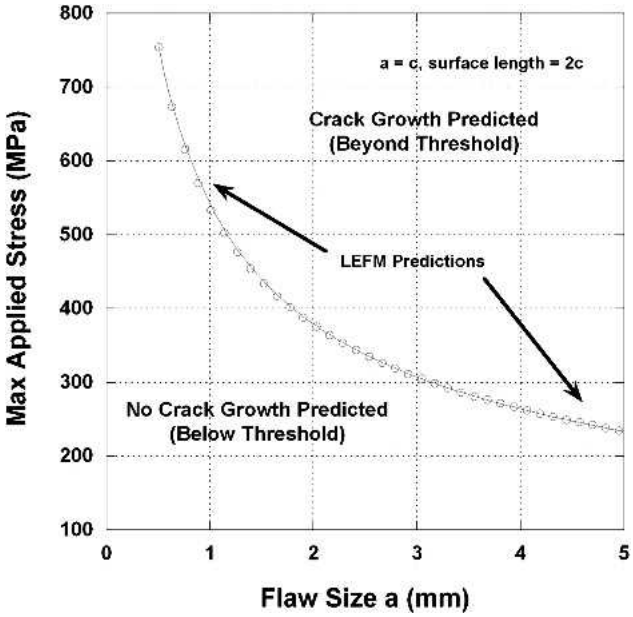

Fig. 6 Example of LEFM predictions for threshold analysis

ing the larger irradiated region can be completed much more quickly than those using a smaller irradiated region. Although the experiments using the smaller irradiated region were useful for determining the spatial distribution of residual stresses inside the shocked region, these experiments were much too time consuming to use extensively. The reason for this is the smaller number of grains satisfying Bragg's law inside the smaller irradiated regions. All further XRD residual stress analysis results were obtained using the larger irradiated region.

3.2.2 In-Depth Residual Stresses Induced by LSP and Conventional Peening. Fig. 5 depicts the surface treatment induced residual stresses used for the life predictions. The depicted curve fits are those used for the numerical computation of the stress intensity factor contribution due to the residual stresses and conform to the functional form of Eq 7.

The compensatory tensile residual stresses required for equilibrium and sometimes found immediately underneath the surface treatment induced compression were not measured and are not considered in the analysis. For the purposes of analysis, the LSP induced compression was assumed to degrade to zero in a linear manner at depths between 1.27 and 1.90 mm.

3.3 Elastic Fracture Mechanics Analysis

Initial attempts were made at life predictions for flawed configurations with and without surface treatment induced compressive residual stresses. Qualitatively, the results were intuitive, with the deep, high magnitude compressive residual stresses yielding either no predicted crack growth or substantially longer propagation lives than specimens without the compressive stresses. The accuracy of these predictions was, however, suspect without experimental validation and none are presented. The reason for this was twofold. First, since peak residual compressive stresses were found at the surface, very often no growth was predicted at the surface in the c direction, while growth was predicted subsurface in the a direction where the residual compression was of lower magnitude. This allowed the *a/c* ratio to grow well beyond 2.0, the limits of the LEFM model. Additionally, in the presence of compressive residual stresses, the total stress ratio R, calculated considering both the applied and residual stresses, was sometimes very highly negative. Calibrating data for the crack growth model was not available for stress ratios $R < -1$. Thus, it was uncertain if the employed crack growth algorithm could provide accurate estimations of crack growth rate for many of the predictions.

With these complications in mind, a more conservative LEFM methodology was employed. Rather than predicting total life to failure, LEFM was employed to conduct a crack growth threshold analysis. In this analysis, the total stress intensity factor range ΔK for the given flaw in the presence of a particular uniform applied stress and residual stress was calculated and compared with the threshold stress intensity factor range. For combinations of flaw geometry and total stress state, plots were composed to visually represent the transition from arrested cracks to growing cracks. This is shown schematically in Fig. 6.

The plots resulting from such an analysis can be found in Fig. 7, 8, 9, and 10 for applied stress ratios $R = 0.1$, 0.5, 0.8, and -1, respectively. Any combination of flaw size a and maximum applied stress falling below the predicted trend line for a given surface treatment is considered to be a design in which no growth is predicted for the flaw.

From these plots the clear advantage of the LSP induced compressive residual stresses was readily apparent. Some threshold benefit is predicted for all four stress ratios, with the magnitude of benefit decreasing with increasing stress ratio. This is due to the relatively smaller impact of the compressive stresses on the total stress intensity factor range at the higher stress ratios. This stress ratio effect has been demonstrated previously for LSP and other deep residual stress inducing surface treatments such as low plasticity burnishing (Ref 28). It is also useful to note that some threshold benefit persists even after the flaw is considerably larger than the induced compressive stresses. This effect was particularly apparent in the case of the LSP induced stresses. These predictions for large flaws

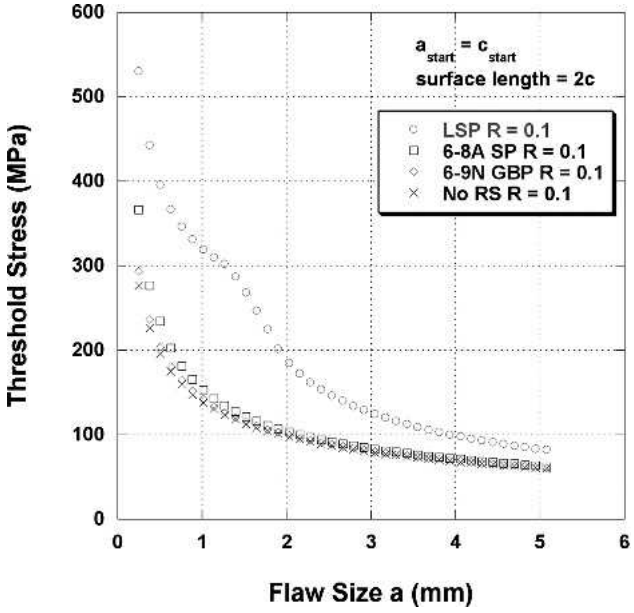

Fig. 7 Max safe applied stress versus flaw size for various surface treatments at applied $R = 0.1$

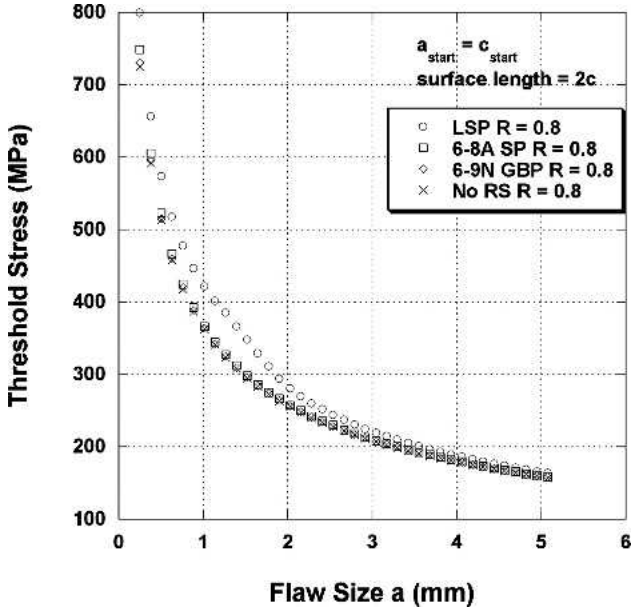

Fig. 9 Max safe applied stress versus flaw size for various surface treatments at applied $R = 0.8$

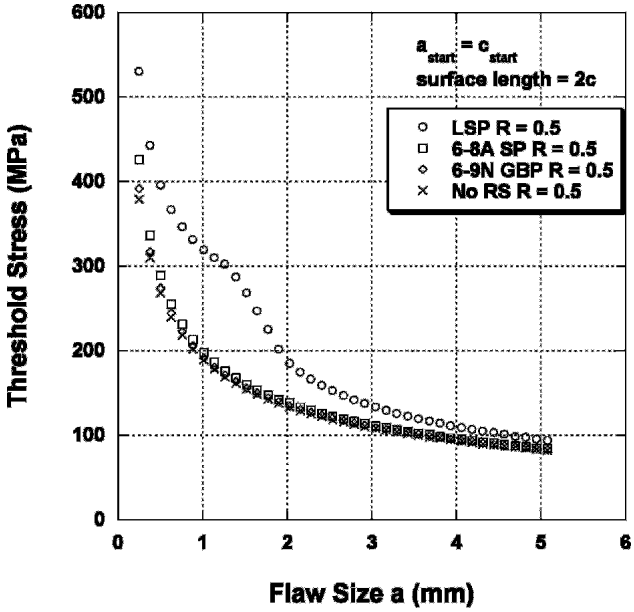

Fig. 8 Max safe applied stress versus flaw size for various surface treatments at applied $R = 0.5$

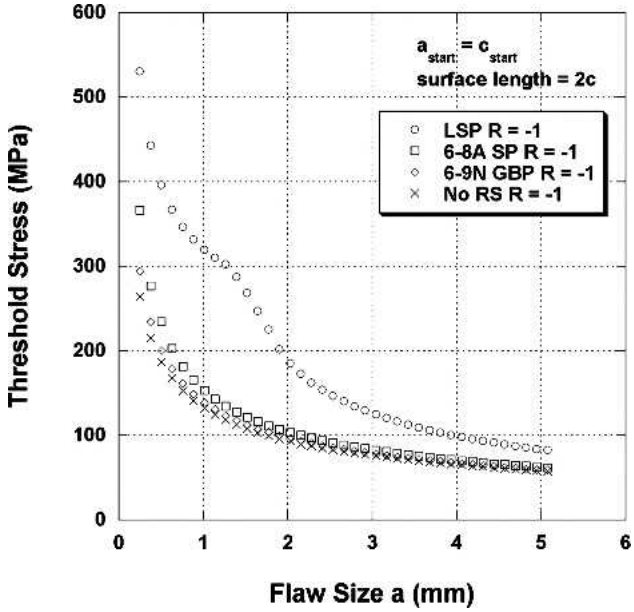

Fig. 10 Max safe applied stress versus flaw size for various surface treatments at applied $R = -1$

are useful for airframe applications where much larger flaws are tolerated than in rotating engine components.

A considerably smaller, but useful, threshold benefit is predicted with the two shot peening conditions considered. The difference in predicted benefit between the shot peening conditions and the LSP condition is due to the rapid extinction of the shot peening induced compressive residual stresses with depth. It should be noted that versus small flaws, which are of primary interest in rotating turbine engine components, the predicted threshold benefit due to conventional peening is substantial.

The differences between threshold predictions at these different stress ratios demonstrates that the magnitude of benefit due to compressive residual stresses, including those induced by LSP will be stress ratio dependent. Thus, when incorporating compressive residual stresses in design, careful consideration will need to be made of the applied load spectrum.

4. Conclusions

The residual stresses induced by high intensity LSP and two variations of conventional shot peening were analyzed in-depth using XRD residual stress analysis. The spatial distribution of surface stresses in an LSP impact was also reported.

A linear elastic fracture mechanics analysis has been used to

predict increases in crack growth threshold performance due to these induced compressive residual stresses. By far, the largest predicted improvement in performance was found with LSP induced stresses. The high relative benefits predicted for LSP are due not just to the magnitude of the LSP induced compressive residual stresses, but also the superior depth of compression. Shot peening induced compressive residual stresses were also predicted to result in an increase in crack growth threshold performance, though the benefit was smaller and of practical use only in the case of small flaws.

The magnitude of the predicted benefit associated with surface treatment induced compression varies with the applied stress ratio R, decreasing with increasing R. As such, careful consideration should be given to the applied loading spectra before any design credit is taken.

References

1. L. Wagner and G. Luetjering, Influence of Shot Peening on the Fatigue Behavior of Titanium Alloys, Proceedings of the 1st International Conference on Shot Peening, (Paris, France), 1981, out of print; full text available at http://www.shotpeening.org
2. A. Niku-Lari, Shot-Peening, Proceedings of the 1st International Conference on Shot Peening, (Paris, France), 1981, out of print; full text available at http://www.shotpeening.org
3. L.H. Burck, C.P. Sullivan, and C.H. Wells, Fatigue of a Glass Bead Blasted Nickel-Base Superalloy, *Metall. Trans.,* Vol 1, 1970, p 1595-1600
4. D. Clarke and S.S. Birley, The Control of Manual Shot Peening, Proceedings of the 1st International Conference on Shot Peening (Paris, France), 1981, out of print; full text available at http://www.shotpeening.org
5. T. Dorr and L. Wagner, Effect of Shot Peening on Residual Life of Fatigue Pre-Damaged 2024 A1, Proceedings of the 6th International Conference on Shot Peening, (San Francisco, CA), 1996, full text available at http://www.shotpeening.org
6. D.M. Corbly, S.R. Mannava, and W.D. Cowie, Application of Laser Shock Peening (LSP) to Titanium Fan Blades, 4th National High Cycle Fatigue Conference, Monterey, CA, 1999
7. A.H. Clauer, D.W. Sokol, D.B. Garcia, L. Bernadel, and R. Ravindranath, Increased fretting fatigue life in laser peened Ti-6Al-4V, 9th National Turbine Engine High Cycle Fatigue Conference (Pinehurst, NC), 2004, full text available at http://www.hcf.utcdayton.com
8. R. Specht, private communication, Metal Improvement Company, Paramus, NJ, May, 2003
9. P. Peyre and R. Fabbro, Laser Shock Processing: A Review of the Physics and Applications, *Opt. Quantum Electron.,* Vol 27, 1995, p 1213-1229
10. A.H. Clauer and D.F. Lahrman, Laser Shock Processing as a Surface Enhancement Process, Proceedings of the Durable Surfaces Symposium, International Mechanical Engineering Congress & Exposition (Orlando, FL) Trans-Tech Publications, Switzerland, 2000 p 121-144
11. C.S. Montross, T. Wei, L. Ye, G. Clark, and Y-W. Mai, Laser Shock Processing and its Effects on Microstructure and Properties of Metal Alloys: A Review. *Int. J. Fatigue,* Vol 24 (No. 10), 2002, p 1021-1036
12. Residual Stress Management by X-ray Diffraction, SAE HS-784. M.E. Hilley, Ed. SAE, Warrendale, PA, 2003
13. I.C. Noyan and J.B. Cohen, *Residual Stress Measurement by Diffraction and Interpretation,* Springer-Verlag, NY, 1987
14. B.D. Cullity, *Elements of X-ray Diffraction,* 2nd ed., Addison-Wesley, Reading, MA, 1978, p 447-476
15. P.S. Prevéy, X-ray Diffraction Residual Stress Techniques, *Metals Handbook,* Vol 10, ASM, Metals Park, OH, 1986, p 380-392
16. D.P. Koistinen and R.E. Marburger, *Trans. ASM,* Vol 67, 1964.
17. M.G. Moore and W.P. Evans, Mathematical Correction for Stress in Removed Layers in X-ray Diffraction Residual Stress Analysis, *SAE Trans.* Vol 66, 1958, p 340-345
18. K.L. Boyd, S. Krishnan, A. Litinov, J.H. Elsner, J.A. Harter, M.M. Rativani, and G. Glinka, Development of Structural Integrity Analysis Technologies for Aging Aircraft Structures: Bonded Composite Patch Repair and Weight Function Methods, Flight Dynamics Directorate, Wright Laboratory, AFMC, 133, WPAFB, OH, 1997
19. G. Glinka and G. Shen, Universal Features of Weight Functions for Cracks in Mode I. *Eng. Fract. Mech.,* Vol 40 (No. 6), 1991, p 1135-1146
20. M. Shiratori, T. Miyoshi, and K. Tanikawa, Analysis of Stress Intensity Factors For Surface Cracks Subjected to Arbitrarily Distributed Surface Stress, *Transactions Jpn. Soc. Mech. Eng. A,* Vol 52 (No. 474), 1986, p 390-398
21. *Stress Intensity Factors Handbook,* Y. Murakami, S. Aoki, et al., Ed., Pergamon Press, Oxford, NY, 1992
22. J.P. Gallagher, R.H. VanStone, et al. Improved High Cycle Fatigue (HCF) Life Prediction. Report # AFRL-ML-WP-TR-2001-4159, WPAFB, OH, AFRL/MLLMN, Materials and Manufacturing Directorate, Air Force Research Laboratory, Air Force Material Command, Wright-Patterson AFB, OH 45433-7750, 2001, p 1158
23. M. Tuft, Shot Peen Impact on Life, Part 3: Development of a Fracture Mechanics/Threshold Behavior Predictive Model, *Proceedings of the 7th International Conference on Shot Peening* (Warsaw, Poland), 1999, out of print; full text available at http://www.shotpeening.org
24. FRANC^{3}D, Cornell Fracture Group, www.cfg.cornell.edu
25. ZENCRACK, Zentech International, Ltd., www.zentech.co.uk zencrack.htm
26. A.H. Clauer, C.T. Walters, and S.C. Ford, The Effects of Laser Shock Processing on the Fatigue Properties of 2024-T3 Aluminum, *Lasers in Materials Processing* (Los Angeles, CA), ASM International, Metals Park, OH, 1983, p 7-22
27. P. Forget, M. Jeandin, and A. Lyaret, Determination of Laser Shock Treatment Conditions for Fatigue Testing of Ni-Based Superalloys. *Suppl. J. Phys. III,* Vol 3, 1993, p 921-928
28. M. Shepard, unpublished research, Air Force Research Laboratory, Materials and Manufacturing Directorate, Wright-Patterson Air Force Base, OH, 2004